Fractal Characterization and Iso-mapping of Parameter Plane of Harmonically Excited Pendulum

Salau, T.A.O.[1] and Olabode, A. A.[2]

Abstract— This study utilized fractal disk dimension characterization to investigate the system response of a nonlinear, harmonically driven pendulum of mass, *m* (or weight, *W*) and length *l* over a well-defined parameter plane of excitation amplitude versus damping factor. The system response was simulated at three drive frequencies (symbol, ω) of 1/3, 2/3 and 3/3. A Runge-Kutta fourth order algorithm, coded in FORTRAN programming language was used to simulate the system response over a 101 by 101 parameter plane with the forcing amplitude (symbol, g) varying between 0.9 and 1.5 and the damping factor (symbol, q) varying between 2.0 and 4.0. Initial conditions for both angular displacement and angular velocity for the simulation at each of the 10,201 points of the plane was set at 0.0 The Poincare section obtained at each node on the parameter plane at the end of 2000 steady-state drive periods was characterized to estimate the fractal disk dimension of the system response at that node. The fractal dimensions of three randomly selected nodes on the parameter plane are returned by computer code. Further, the nodes whose fractal dimensions are within an upper and lower tolerance of 1% of the fractal dimensions of these randomly selected nodes are also returned by code and they, along with the random fractal dimensions of the three randomly selected nodes are plotted on the parameter plane in the form of an equal potential (system response) plot. This plotting on the parameter plane to show the points that correspond to each of the three bands is done in order to achieve the iso-mapping on the plane. The steady-state response of a nonlinear, harmonically driven system depends on the drive frequency, the forcing amplitude and the damping factor. With a lower drive frequency of 1/3, higher fractal dimensions (above 1.0) were obtained with a combination of high damping factor and low to medium forcing amplitude; with the median drive frequency of 2/3, fractal dimensions above 1.0 were obtained with a combination of low damping factor and medium to high forcing amplitude; while with the higher drive frequency of 3/3, a fractal dimension that is up to 1.0 was not obtainable at any of the 10,201 nodes on the parameter plane. We note that as the forcing amplitude is increased from 0.9, in order to assure early onset (as from g=1.044) of higher fractal dimensions that are above 1.0, lower drive frequency (1/3) must be used. The results of this study could be used for engineering design, education and fashion design.

Index Terms— Damping factor, Forcing amplitude, Fractal disk dimension, Nonlinear pendulum, Parameter plane, Poincare section, Runge-Kutta, System response.

1 Introduction

THE pendulum has established itself as a test piece both for the exemplification and study of linear and nonlinear vibratory systems. Since the first observations of Galileo, many researchers have likewise used it to study vibration in its many forms. This research work toes the same line in the study of the response of a nonlinear pendulum to varying combinations of forcing amplitude and damping over a large 101 by 101 (that is 10,201-point) parameter plane with the forcing frequency held constant. The observation and fractal characterization of this response, which may be chaotic since the necessary conditions for chaos, namely nonlinearity among at least three independent dynamical variables (angular displacement, angular velocity and time) [1] are present in the system, over a parameter plane of parameter combination points to get corresponding fractal dimensions and the iso-mapping (of similar dimension values) over this parameter plane, is the objective of this research work. A fractal is an object that displays self similarity on all scales. A plot of the quantity on a log-log graph of count versus scale then gives a straight line, whose slope is the fractal dimension. The harmonically excited pendulum is one that is driven by a sinusoidally varying load and the system's response could be periodic, quasi-periodic or chaotic. The term chaos has been described as sensitivity to small differences in initial conditions [1]. When the response is chaotic, it could be studied by differing methods or visual tools and an example of this is the Poincaré section. For chaotic response the section is a fractal shape.

A fractal possesses self similarity across a range of spatial scales and, not having integer dimensions like Euclidean objects, can be described by its ability to fill the Euclidean space in which it is embedded [2], [3], [4], [5], [21]. Thus fractal dimensioning can handle all shapes regardless of complexity. Fractals are highly employed in computer modelling of irregular patterns and structures in nature. Although the theory of chaos and the concept of fractals evolved independently, they have been found to penetrate each other's fronts. Although the orbits of nonlinear dynamical systems could be attracted or repelled to simple shapes of nonlinear, near-circles or other shapes of Euclid, these are rare exceptions and the behaviour of most nonlinear dynamical systems tends to be more complicated [4], [6]. The analysis of nonlinear dynamics fractals is useful for obtaining information about the future behaviour of complex systems because they provide fundamental knowledge about the relationship between these systems and uncertainty and indeterminism; in addition, the dimension of Poincaré recurrences may serve as an indicator of the onset of synchronized chaotic oscillations and thus researchers have established the utility of fractal dimensioning as an effective characterization tool [7], [8], [4]. Chaotic dynamical systems with phase space symmetries do exhibit riddle basins of at-

traction that can be viewed as extreme fractal structures not minding how infinitesimal the uncertainty in the determination of an initial condition and it is not possible to decrease the fraction of such points that will surely converge to a given attractor [9]. Some of the visual tools that enrich the understanding of chaotic behaviour include state variables (time series), the phase portrait, the Poincaré map, the power spectrum, the Lyapunov exponents and bifurcation diagram [10]. The bifurcation and chaos behaviour of horizontal platform system (HPS), used in offshore and earthquake technology, and in a 4-sided simply supported rectangular thin electromagneto-elastic plate in electromagnetic, mechanical and temperature fields have been studied [11], [12]. Narayanan and Jayaraman [16] emphasized that one of the major ways to investigate the dynamics of continuous time system by differential equations was the use of Runge-Kutta methods in developing bifurcation diagram and a critical review of Runge-Kutta discontinuous Galerkin (RGDK) methods for nonlinear convection dominated problems which has become a breakthrough in computational fluid dynamics especially in producing its chaos diagrams was carried out by [13]. The RKDG methods review also showed its immense applications in Navier-Stokes equations and Hamilton-Jacobian equations. Also the chaotic behaviour of a transformer during ferro-resonance under single and double-open conductor configurations and the solutions of the nonlinear differential equations, using Runge-Kutta fourth order method categorized the behaviour into periodic, quasi-periodic, and chaotic types. The results which were corroborated using Electro Magnetic Transients Program (EMTP) showed the influence of parameters (i.e. transformer saturation characteristic, core loss, and the amplitude of the voltage source) on the system response [14]. Chaotic vibrations of a harmonically excited non-linear oscillator with coulomb damping was investigated in a range of excitation frequencies with the observation of a period doubling route to chaos in certain frequency ranges [15]. An improvement in the characterization of surface finish of machined surfaces was obtained through the use of fractal analysis [17] while the analysis of the corrosion fronts of aluminium foils in an experimental investigation showed that the fronts can be described in terms of self-affine fractal geometry over a significant range of length scales [18]. The use of multifractal scaling of pore volume as a tool for rock characterization to demonstrate that a certain amount of order can be extracted from an apparently random distribution of pores in sedimentary rock was done by [19] while it has been shown [20] by atomic force microscopy (AFM) method that the surface characteristics of a film of Indium Tin Oxide (ITO) annealed at high temperatures (300°C) has higher surface roughness with the fractal dimension, calculated by the height-height correlation function, of the surface falling between 2.15 and 2.19, depending on the annealing temperature. Fractal analysis was used [22] to study the various harmonic current waveforms generated by typical nonlinear loads The gap that this study intends to fill through the use of Runge-Kutta fourth order simulations using a Fortan-90 coded computer program is to characterize and make a plot of equal potential points covering a well defined parameter range consisting of 10,201 parameter combination points This work takes advantage of the fact that computers are good at repetitive tasks with high precision and speed beyond human capability.

- *Salau Tajudeen Abiola Ogunniyi is a senior lecturer in the department of Mechanical Engineering, University of Ibadan (currently on Sabbatical at Ladoke Akintola University of Technology, Ogbomoso) both in Nigeria. By dint of hard work, he was promoted Lecturer I in2002 and senior Lecturer in 2008. His specialization is in solid mechanics with bias for nonlinear dynamics and chaos. E-mail: tao.salau @ui.edu.ng*
- *Olabode Ayodele Akangbe is currently pursuing masters degree program in mechanical engineering in Ladoke Akintola University of Technology, Ogbomoso, Nigeria. He is currently an employee of Chevron Nigeria Limited. He is interested in fluid dynamics and energy studies. E-mail: aolabode@chevron.com*

2 Theory and Methodology

2.1 Theory

The governing equation for the damped, sinusoidally driven nonlinear pendulum of mass m (or weight W) and length l is given by:

$$m l d^2\theta/dt^2 + \gamma d\theta/dt + W \sin\theta = A\cos(\omega_D t) \quad (1)$$

where the various terms on the left represent acceleration, damping and gravitation. Expressed in dimensionless form, in order to minimize the number of adjustable parameters, (1) becomes:

$$d^2\theta/dt^2 + 1/q\,(d\theta/dt) + \sin(\theta) = g\cos(\omega_D t) \quad (2)$$

Where q is the damping factor or quality parameter, g is the forcing amplitude and ω_D is the drive frequency.

From [23], (2) may be transformed (taking Θ_1 as angular displacement and Θ_2 as angular velocity) into a pair of first order differential equations to obtain

$$d\theta_1/dt = \theta_2 \quad (3)$$

$$d\theta_2/dt = g\cos(\omega_D t) - (1/q)\theta_2 - \sin(\theta_1) \quad (4)$$

According to literature, research interest focuses on the q- and g-ranges defined by $2.0 \le q \le 4.0$ *and* $0.9 \le g \le 1.5$

2.2 Simulation

The original parameter plane before the commencement of the simulations is shown in Fig. 1.

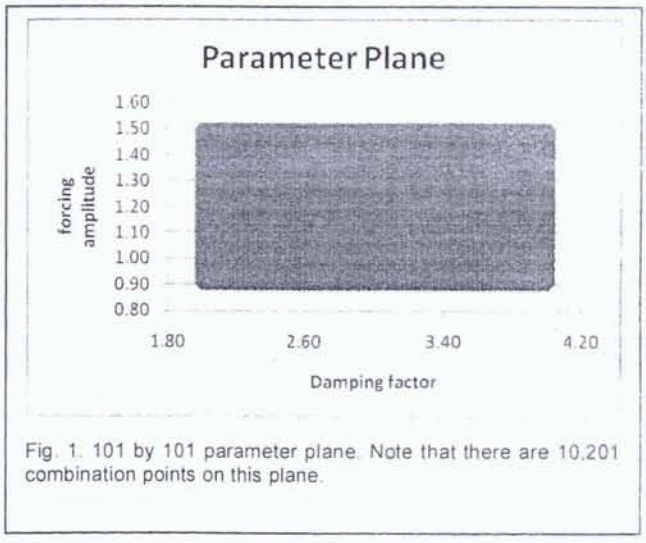

Fig. 1. 101 by 101 parameter plane. Note that there are 10,201 combination points on this plane.

As noted earlier, the value of the damping parameter varies from 2.0 to 4.0 subdivided into 100 places to give 101 divisions. The value of forcing amplitude similarly, is in 101 divisions and is varied from 0.9 to 1.5. In order to simulate the response of the system given by (1), a Runge-Kutta fourth-order algorithm coded in Fortran 90 computer language is employed to simulatenously solve (3) and (4). This computer programme ran on a 32-bit Windows Vista Operating System on a HP-Compaq laptop. The solutions of the angular displacements and velocities obtained at the end of each drive period are tracked with only the steady state solutions retained in order to obtain data for the Poincare section. 500 computations of angular displacement and velocity are computed within each drive period. 2000 steady state solutions of angular displacement and angular velocity are in this way stroboscopically obtained at each combination point on the parameter plane and used to construct the Poincare section for that point.

A base drive frequency of 2/3 was used in the first instance to drive over the entire parameter plane and subsequently the drive frequency was varied first to 1/3 and then to 3/3 =1.0. Following the procedure in [4], the Poincare section obtained after simulating at each point on the parameter plane is analyzed using fractal disk dimensioning method to obtain the fractal dimension. The 10,201 fractal dimensions produced over the entire parameter plane are then distributed over a 100 equal-width distribution. The fractal dimensions of three randomly selected nodes on the parameter plane are returned by computer code. Further, the nodes whose fractal dimensions are within an upper and lower tolerance of 1% of the randomly selected fractal dimensions of these nodes are also returned by code and they, along with the random fractal dimensions of the three randomly selected nodes are plotted on the parameter plane in the form of an equal potential (that is, system response) plot. All random number generation in this work was done with a seed value of 9876.

Compactly expressed in flow chart form the method followed in this study is shown in Fig. 2.

To characterize the fractals obtained at each node on the parameter plane, we followed the procedure in [4]. The fractal dimension of all the 10,201 points on the parameter plane are in this manner obtained and track kept of the values of all of them. Following this the collection of 10,201 fractal dimensions are sorted from lowest to highest and the sorted collection arranged into an equal-width, 100-range distribution. The analysis of the program output data and the construction of the iso-mapping of fractal dimensions on the parameter plane was carried out using Microsoft Office Excel 2007 running on 32-bit Windows Vista Operating System on a HP-Compaq laptop.

3 Results and Discussion

3.1 Results

Simulating over the entire parameter plane with ω=2/3 to obtain the fractal dimension at each of the 10,201 points gave the lowest fractal dimension as 0.0000 and the highest fractal dimension as 1.3671 (both to 4 decimal places). After spreading the fractal dimensions (from lowest to highest) over a 100 equal-width distribution and taking note of the count of points within each range, we obtain that the range with the highest population or count of points within it to be the 1st range bounded between 0.0000 and 0.0137, with a modal value of 0.0068. This range contained 3,143 out of the total 10,201 points or 30.811%. One range, the 2nd range, (0.0137 to 0.0273, with modal value of 0.0205) contained no points at all.

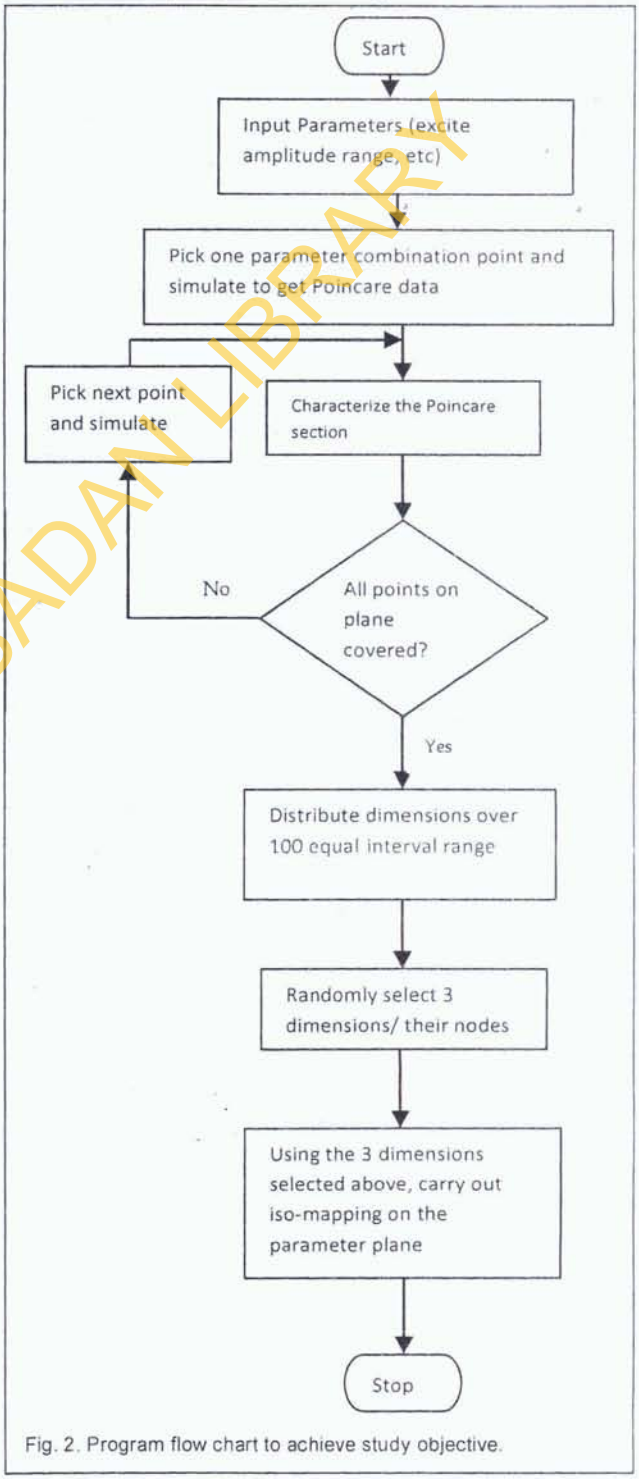

Fig. 2. Program flow chart to achieve study objective.

The next highest populated range after the 1st range is the 10th range (0.1230 to 0.1367, with modal value of 0.1299) with 360 (3.529%) points within it. Between the 1st and 10th ranges, the number of points per range was always below 100 (0.980%).

Also after the 10th range, the count of points per range fell again to below 100 until the 80th range which had a count of 122 points while the count remained above 100 points from the 80th range all through to the 95th range which had a count of 153 points. From the 96th range to the 100th range the count fell and remained below 100 with the 100th range having a count of 4 points. This result is shown graphically in Fig. 3.

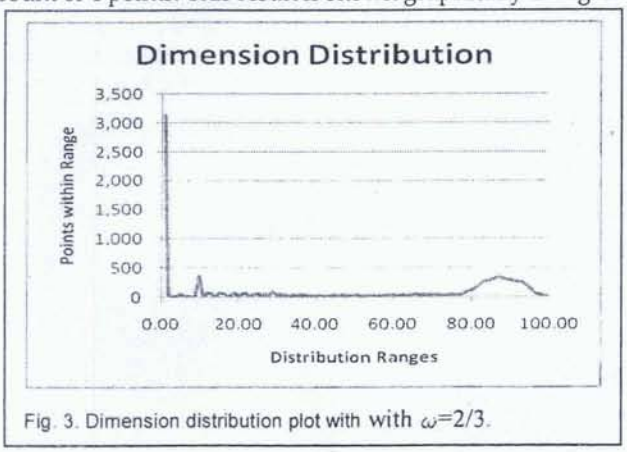

Fig. 3. Dimension distribution plot with with ω=2/3.

Repeating the simulation over the parameter plane with ω=1/3 gave the lowest fractal dimension as 0.0000 and the highest as 1.3819 (both to 4 decimal places). After spreading the fractal dimensions (from lowest to highest) over a 100 equal-width distribution and taking note of the count of points within each range, the range with the highest population was the 1st range bounded between 0.0000 and 0.0139, with a modal value of 0.0069. This range contained 3,951 out of the total 10,201 points or 38.731%. Five ranges (the 2nd, 3rd, 8th, 12th and 14th ranges) contained no points at all. The next highest populated range after the 1st range is the 89th range (1.2222 to 1.2360, with modal value of 1.2291) having 480 (4.705%) points within it. Between the 1st and 82nd ranges, the number of points per range was always below 100 (0.980%). From the 83rd range up to the 96th range the count of points per range remained above 100 but from the 97th range, it fell again to below 100 and remained so until the 100th range having a count of 2 points. This result is shown graphically in Fig. 4.

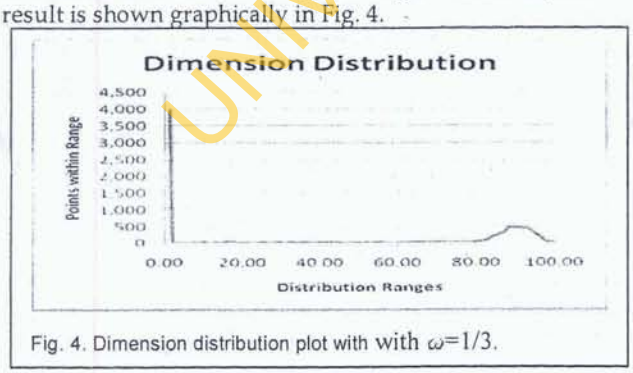

Fig. 4. Dimension distribution plot with with ω=1/3.

Finally, repeating the simulation over the parameter plane with ω=3/3 gave the lowest fractal dimension as 0.0000 and the highest fractal dimension as 0.8192 (both to 4 decimal places). After spreading the fractal dimensions (from lowest to highest) over a 100 equal-width distribution and taking note of the count of points within each range, the range with the highest population was again the 1st range bounded between 0.0000 and 0.0082, with a modal value of 0.0041. This range contained a vast 10,012 out of the total 10,201 points or 98.147%. More than half of the ranges in the distribution (53 out of 100) contained no points at all. The next highest populated range after the 1st range is the 16th range (0.1229 to 0.1311, with modal value of 0.1270) having 104 (1.020%) points within it. All the remaining ranges apart from the 83rd range had a count of points below 5. By the way, the 83rd range itself had exactly 5 points within it. The 100th range had a count of 1 point. This result is shown graphically in Fig. 5.

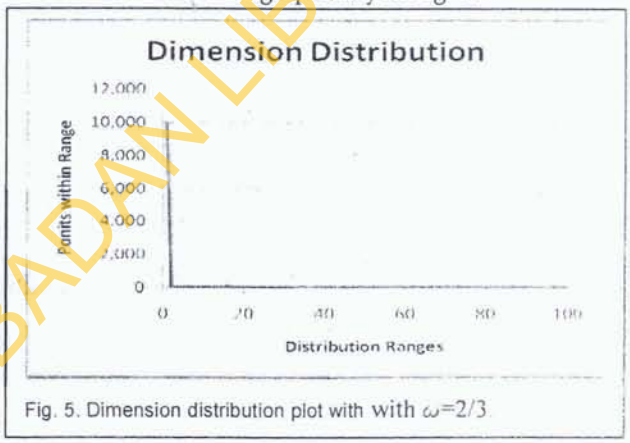

Fig. 5. Dimension distribution plot with with ω=2/3

Further, with ω=1/3, the random selection code returned the three fractal dimensions 0.0000, 1.2975 and 0.0000 with the total number of unique points with fractal dimension within 1% tolerance of their values equalling 4,632. Plotting this number of points on the parameter plane along with the random dimensions that returned them gave the plot in Fig. 6.

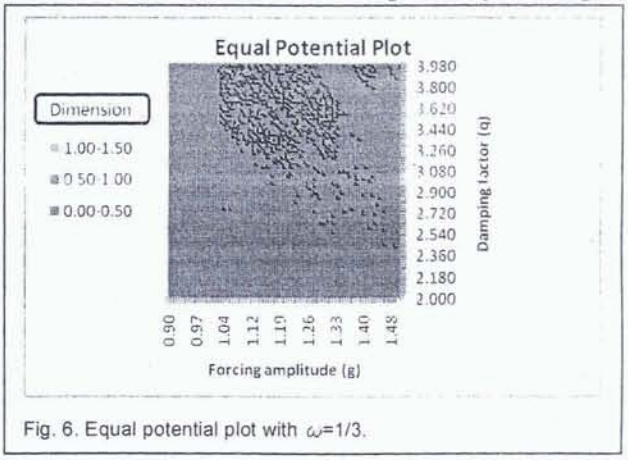

Fig. 6. Equal potential plot with ω=1/3.

From Fig. 6, the dimensions of the different points on the pa-

rameter plane could of three types represented by colour codes, with green standing for 1.0 to 1.5 fractal dimension, reddish brown standing for 0.5 to 1.0 fractal dimension and blue standing for 0.0 to 0.5 fractal dimension. A first, cursory look at Fig. 6 would suggest that the figure is a scatter plot of forcing amplitude against damping factor. However, noting that this plot is made on a 101X101 paramter plane containing 10,201 nodes which would drastically squeeze the points into a very small space thus leading to the omission of useful detail, and also recalling that this plot is made, not with the scatter plot feature, but rather the surface plotting feature of Microsoft Excel 2007 with the specification to do a contour plot, we dig deeper by magnifiying to unravel hidden detail. Viewing at the maximum resolution of 400% in Microsoft Excel 2007, a small part (we can no longer see the whole figure at once) of Fig. 6 is shown in Fig. 7.

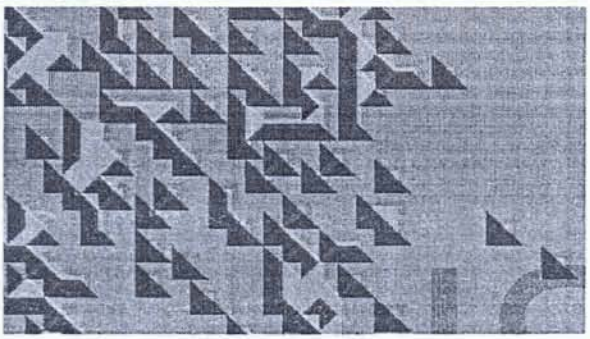

Fig. 7. A small part of Fig.6 viewed at 400% magnification.

As the shapes in Fig. 7 confirm, the apparent dots in Fig. 6 are actually not dots but rather are a series of approximate concentric figures, occasionally rectangular but mostly irregular, with different colour bands-green at the centre (1.0 to 1.5 fractal dimension), reddish brown in the middle band (0.5 to 1.0 fractal dimension) and blue at the outermost band (0.0 to 0.5 fractal dimension). Also all these colour bands close up completely forming contours of points with similar fractal dimensions Each coloured band denotes the fractal dimension of the points that it covers while the size or area of the band gives an indication of the number of points contained within it.

Continuing with Fig. 6, we see that there is a concentrated cluster of points within the region bounded by damping factor = 3.120 to 4.000 and forcing amplitude = 1.020 to 1.356 with the innermost green band (fractal dimension = 1.0 to 1.5) increasing in area as the value of the forcing amplitude decreases and the damping factor increases. However, we also note that as the forcing amplitude increases and the damping factor decreases, the area of the innermost green band shrinks but there is no occurrence on the parameter plane where the green innermost area disappears altogether. Away from the large concentrated cluster of points on the parameter plane, and towards the bottom right region of Fig. 6 the contours become less concentrated, spreading out, with the areas of the reddish brown band and the blue band increasing relative to that of the green band. The same is true of the very small cluster in the top right corner of the figure although in keeping with our earlier observation, the area of the green band increased as the damping factor increased towards 4.000. Within the large cluster dominating the equal potential plot, and possibly for the whole figure, the sum total area of green (fractal dimension from 1.0 to 1.5) bands is more than either that of the reddish-brown (fractal dimension from 0.5 to 1.0) bands or the blue (fractal dimension from 0.0 to 0.5) bands.

With the drive frequency changed to $\omega=2/3$, the random selection code returned the three fractal dimensions 1.0926, 0.0000 and 0.3795 with the total number of unique points with fractal dimension within 1% tolerance of their values equalling 246. Plotting this number of points on the parameter plane along with the random dimensions that returned them gave the plot in Fig. 8.

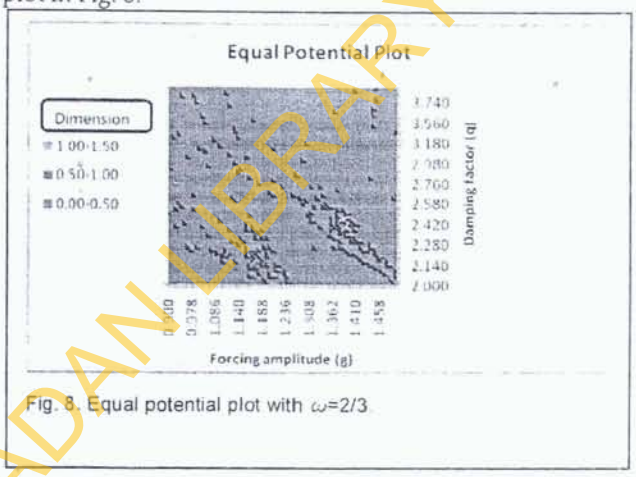

Fig. 8. Equal potential plot with $\omega=2/3$

As noted earlier, what we have in Fig. 8 are not dots but rather are a series of approximate concentric bands. There are occasions with $\omega=2/3$ when the two inner colour bands of green and reddish-brown are entirely crowded out by the outer blue band. Curiously however, whenever the middle reddish-brown band is present, the innermost green band is always retained, no matter how small the area it covers. While this may not be readily apparent looking at Fig. 8, it becomes very glaring at the maximum magnification of 400%.

In the arrangements of the contour bands on the parameter plane, there is a change in pattern from when $\omega=1/3$. The concentrated cluster of points has moved from the upper part of the parameter plane to the lower part while at the same time the clusters are now two, with the larger one in the bottom right region of the plotted parameter plane. Within the bottom-right cluster (damping factor = 2.000 to 2.620 and forcing amplitude = 1.248 to 1.500), the areas of the innermost green bands increased with increasing damping factors and decreasing forcing amplitudes, although overall the total area of the middle reddish-brown bands is more than either that of the green bands or the blue bands. This same observation holds true for the bottom-middle cluster (damping factor = 2.000 to 2.300 and forcing amplitude = 1.104 to 1.248). Away from these two clusters at the bottom of the parameter plane, the remaining colour bands are more pronouncedly spread out than for the case when $\omega=1/3$. However, even with the spread out, the sum total area of reddish-brown (fractal dimension from 0.5 to 1.0) bands are more than either that of the green (fractal dimension from 1.0 to 1.5) bands or the blue (fractal

dimension from 0.0 to 0.5) bands. In addition, we note that there is a substantial number of colour contours that are filled entirely with the outermost blue (fractal dimension from 0.0 to 0.5) band, thus crowding out both the middle reddish-brown (fractal dimension from 0.5 to 1.0) bands and the innermost green (fractal dimension from 1.0 to 1.5) bands but these contours are not in the majority on the equal potential plot on the parameter plane for the case when ω=2/3. Curiously, there are no contours filled entirely with the reddish-brown band, although some are very nearly so filled. A detailed look at 400% magnification reveals that whenever the reddish-brown bands appear, the innermost green band is always retained, even if it is actually very small in area.

When the drive frequency was changed to ω=3/3, the random selection code returned the three fractal dimensions 0.0000, 0.0000 and 0.0000 with the total number of nodes that give fractal dimensions that are within 1% tolerance of them equalling 9,923. This is not entirely a surprise since the probability of getting a fractal dimension of 0.0000 with this drive frequency is more than 0.98 (almost unity!). Plotting this number of points on the parameter plane along with the randomly selected fractal dimensions that was used to extract them gave the plot in Fig. 9.

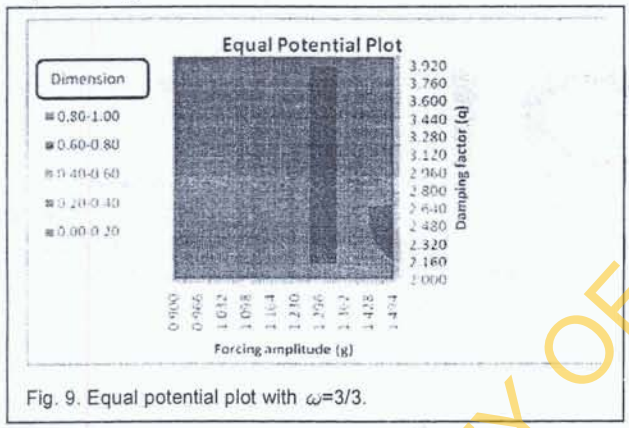

Fig. 9. Equal potential plot with ω=3/3.

The number of points on the parameter plane in Fig. 9 is more than 9,000 with all of their fractal dimensions equal to 0.0000. Noting that the colour code for fractal dimension 0.0000 is blue, it is not surprising that the entire parameter plane is covered in blue. All the points on this plane have a fractal dimension of 0.0000. Viewing at higher magnifications up to the maximum of 400% yields no further graphic detail.

3.2 Discussion

The highest dimension obtained throughout the simulations was 1.3819 which was obtained with a drive frequency of ω=1/3. The lowest fractal dimensions obtained while simulating on the parameter plane for the three cases of ω used was always 0.0000, while the highest fractal dimensions obtained were respectively 1.3819 for ω=1/3, 1.3671 for ω=2/3 and 0.8192 for ω=3/3, suggesting an inverse variation between the value of drive frequency (ω) used and the maximum obtainable fractal dimension when simulating over the parameter plane. In addition, for all ω-cases, the majority of the fractal dimensions obtained at the points was always 0.0000 (38.731% for ω=1/3, 30.811% for ω=2/3 and 98.147% for ω=3/3), although this did not follow a discernible pattern and hence no relationship between drive frequency (ω) and the percentage of points with 0.0000 fractal dimension is suggested here. On the equal-width range distribution, out of the 100 ranges, the number of ranges that contain no point on the parameter plane is respectively, 5 for ω=1/3, 1 for ω=2/3 and 53 for ω=3/3. This also follows no ready pattern and hence prediction is impossible in this regard.

For the case when ω=1/3, looking at Fig.6, we note that the collection of points with high fractal dimensions (1.0 to 1.5) occur in larger numbers in the top half region, in the area defined by forcing amplitude (g) =1.020 to 1.356 and damping factor (q) =3.120 to 4.000. The collection of points with higher fractal dimensions (1.0 to 1.5) are surrounded by points with median fractal dimensions (0.5 to 1.0) which are also in turn surrounded by points with even lower fractal dimensions (0.0 to 0.5). The above suggests that with ω=1/3, higher fractal dimensions will be readily obtained by a combination of high damping factor and low to medium forcing amplitude. In addition, within this large cluster in Fig.6, there is a general propensity for the areas of the green (high fractal dimension) bands to increase as the damping factor increases and the forcing amplitude decreases. On the parameter plane, when ω=1/3, the large green coloured bands (fractal dimension greater than 1.0) start to occur as early as forcing amplitude (g) =1.044 and fall off after 1.368.

For the case when ω=2/3, looking at Fig.8, the equal potential plot contained two sizable clusters instead of one (that we had with ω=1/3), and now also the position of the clusters is shifted to the lower region of the figure. The larger cluster in the bottom-right corner is within the area defined by forcing amplitude (g) =1.248 to 1.500 and damping factor (q) =2.000 to 2.620, while the second cluster is in the mid-bottom to bottom-left area defined by forcing amplitude (g) =1.056 to 1.248 and damping factor (q) =2.000 to 2.400. Within these two clusters, the area of the parameter plane covered by the green contour bands (fractal dimension greater than 1.0) is substantial although the overall total area covered by the reddish-brown contour bands is still the majority. In addition, within these two clusters, generally, the area of the green coloured contour bands is increased by increasing damping factor and reducing forcing amplitude. However, with ω=2/3, the value of forcing amplitude required to obtain a fractal dimension above 1.0 is generally higher (1.104 to 1.448 as against 1.044 to 1.368 for when ω=1/3). Within the second cluster of points in the middle bottom to bottom left area of the parameter plane, if the damping factor is held constant with the forcing amplitude allowed to decrease, the number of points with fractal dimension greater than 1.0 increase. At the top right corner of the parameter plane where the damping factor is highest but with accompanying high values of forcing frequency, the points almost exclusively give a fractal dimension that is between 0.5 and 1.0 while at the bottom left corner existing points exclusively give a fractal dimension that is less than 1.0.

For the case when ω=3/3, looking at Fig.9, the equal potential plot is all blue indicating fractal dimension that is all 0.0000 for the plot of the points that gave the three randomly

selected fractal dimensions along with the points having fractal dimensions that are within a tolerance of 1% of them.

4 Conclusion

This study has demonstrated that the three adjustable parameters of the non-dimensionalized damped, sinusoidally driven non-linear pendulum (the drive frequency, the forcing amplitude and the damping factor) exert pronounced effects on the steady state response of the system (as determined by fractal dimension). With drive frequency of 1/3, fractal dimension greater than 1.0 is obtained with a combination of high damping factor and low to medium forcing amplitude; with a drive frequency of 2/3, fractal dimension greater than 1.0 is obtained by a combination of low damping factor and medium to high forcing amplitude whereas with a drive frequency of 3/3, it is not possible to obtain a fractal dimension that is up to 1.0. Generally, the numbers of nodes that have fractal dimension greater than 1.0 increase with increasing damping factor and decreasing forcing amplitude. Particularly, when the drive frequency is 1/3, nodes whose fractal dimension is greater than 1.0 occur more readily above q=3.120 and the onset of these high fractal dimensions start early as g is increased from 0.9 (around g=1.044) while for drive frequency of 2/3, they occur below q=2.620 and their onset start later (around g=1.104). All over the iso-mapped parameter plane, nodes or points that have the same colour code can be used interchangably to obtain fractal dimensions corresponding to the colour (blue for 0.0-0.5, reddish-brown for 0.5-1.0 and green for 1.0-1.5). The results of this study could be applied in the design of harmonically driven nonlinear engineering systems that are to have a desired degree (or absence) of chaotic response. It could also be used in the field of technical and engineering instruction or education that pertain to the vibration response of nonlinear dynamical systems. The interesting plot of the iso-mapped parameter plane for the cases when ω=1/3 and 2/3 could be used in aesthetic fashion design.

References

[1] Gregory, L.B. and Jerry, P.J., 1990. Chaotic Dynamics: An Introduction. Cambridge University Press, New York, ISBN 0-521-38258-0 Hardback, ISBN 0-521-38897-X Paperback.

[2] Feder, J., 1988. Fractals. Plenum Press, New York.

[3] Mandelbrot, B.B., 1983. The fractal geometry of nature. Freeman, New York.

[4] Salau, T.A.O. and Ajide, O.O., 2012(a). Fractal Characterization of Evolving Trajectories of Duffing Oscillator. International Journal of Advances in Engineering & Technology (IJAET), Vol. 2, Issue 1, pg 62-72.

[5] Oldřich, Z., Michal, V., Martin, N. and Miroslav, B., 2001. Fractal Analysis of Image Structures. Harfa-Harmonic and Fractal Image Analysis, Pg. http://www.fch.vutbr.cz/lectures/imagessci/harfa.htm

[6] Salau, T.A.O., 2002. Fractal analyses and characterization of tread patterns of automobile tyres. Unpublished Doctor of philosophy (PhD) Thesis. Mechanical Engineering Department, University of Ibadan, Nigeria.

[7] Jacobo, A., Ricardo, L.V. and Miguel, A.F.S., 2009. Fractal structures in nonlinear dynamics. American Physical Society's New Journal. Vol. 81, Issue 1.

[8] Valentine, S.A., Wen-Wei, L. and Nikolai, F.R., 2000. Fractal dimension for Poincare recurrences as an indicator of synchronized chaotic regimes. International journal of bifurcation and chaos. Vol. 10 No. 10.2323-2337. World scientific publishing company

[9] Carmago, S., Lopes, S.R. and Viana, 2010. Extreme fractal structures in chaotic mechanical systems: Riddled basins attractor. XI Latin American Workshop on nonlinear phenomena. Journal of physics: Conference series 246 (2010) 012001. Doi:10.1088/1742-6596/24611/012001. IOP publishing Ltd.

[10] Özer, A.B. and Akin, E., 2005. Tools for detecting chaos, SAÜ Fen Bilimleri Enstitüsü Dergisi. Cilt, 1. Sayõ 2005, Pg 60-66, Fırat Üniv. Müh. Fak. Bilgisayar Müh. Böl. ELAZIĞ.

[11] Wang, C.C., Pai, N.S., Yau, H.T., Liao, T.T., Jang, M.J., Lee, C.W. and Hong, W.M., 2010. Bifurcation analysis of horizontal platform system. World Academy of Science, Engineering and Technology, Vol 65 Pg. 1062-1065.

[12] Wei, G. Z. and Xiang, Z. B., 2010. Bifurcation and Chaos of a 4-Sided Simply Supported Simply Supported Thin Electro-Magneto-Elastic Plate in Many Fields. Journal of Advanced Materials Research, Manufacturing Science and Engineering, Pg. 442-448.

[13] Bernardo, C. and Chi-Wang, S., 2011. Runge-Kutta Discontinuous Galerkin Methods for Convection Dominated Problems. Journal of Scientific Computing, Vol. 16, No. 3.

[14] Al-Anbarri, K., Ramanujam, R., Subba-Rao, C. H. and Kuppusamy, K., 2002. Effect of Circuit Configurations on Chaotic Ferroresonance in a Power Transformer, Electric Power Components and Systems, Taylor and Francis, Vol. 30, Issue 10, Pg. 1015-1031. DOI: 10.1080/15325000290085334.

[15] Narayanan, S. and Jayaraman, K., 2003. Chaotic Vibration in a nonlinear oscillator with Coulomb Damping, Journal of Sound and Vibration, Elsevier, Vol.146, Issue 1, Pg. 17-31.

[16] Narayanan, S. and Jayaraman, K., 1989. Control of Chaotic Oscillations by Vibration Absorber ASME Design Technical Conference, 12th Biennial Conference on Mechanical Vibration and Noise. DE 18.5, 391-394.

[17] Alabi, B., Salau, T.A.O. and Oke, S.A., 2007, Surface Finish Quality Characterization of Machined Work Pieces Using Fractal Analysis. MECHANIKA, Nr. 2(64), Pg. 65-71, ISSN 1392-1207.

[18] Terje, H., Torsein, J., Pau, M. and Jens, F., 1994. Fractal Characterization of Two-Dimensional Aluminium Corrosion Fronts. APS Journals, Physical Review E50, Pg. 754-759. © 1994 The American Physical Society.

[19] Muller, J. and McCauley, J.L., 1992. Implication of fractal geometry for fluid flow properties of sedimentary rock. Transport in porous Media, June 1992, Vol. 8, Issue 2, Pg. 133-147.

[20] Davood, R., Ahmad, K., Hamid, R.F. and Amir, S.H.R., 2007. Surface Characterization and Microstructure of ITO Thin Films at Different Annealing Temperatures. Elsevier: Applied Surface Science, Vol. 253, Pg.9085-9090, Science Direct. www.elsevier.com/locate/apsusc

[21] Shu-zu, L. and Angus, H., 1996. Fractal Analysis to Describe Irregular Microstructures. Journal of the Minerals, Metals and Materials Society. Vol. 47, No. 12, Pg. 14-17.

[22] Kingsley, C.U., Azah, M., Aini, H. and Ramizi, M., 2004. The use of Fractals for Characterizing Nonlinear Load Harmonics. Iranian Journal of Electrical and Computer Engineering, Vol. 3, No.2.

[23] Kim Gaik Tay, et al, 2012. A Spreadsheet Solution of a System of Ordinary Differential Equations Using Fourth-Order Runge-Kutta Method. Spreadsheets in Education (eJSiE), Vol. 5, Issue 2